

Imaging bone structure and osteoporosis using MRI

**Sandra J. Shefelbine
Sharmila Majumdar**

Musculoskeletal and Quantitative Imaging Research
Department of Radiology
University of California, San Francisco, CA, USA

Address for correspondence:
Sharmila Majumdar, Ph.D.

Director Musculoskeletal and Quantitative Imaging Research Group (MQIR), Professor Dept. of Radiology, UCSF, Professor Depts. of Orthopedic Surgery & Growth and Development UCSF and Dept. of Bioengineering UC Berkeley, Campus Box 2520
University of California, San Francisco
QB3 Building, 2nd Floor, 203D
1700 - 4th Street
San Francisco, CA 94158, USA
Ph. +1 415 476-6830 and 415 353-4534
Fax +1 415 514 9656
E-mail: sharmila.majumdar@radiology.ucsf.edu

Summary

In addition to Bone Mineral Density (BMD) bone quality plays an important role in defining bone strength. Trabecular bone quality can potentially be defined by several factors, for example trabecular micro-architecture, matrix composition of trabeculae and trabecular bone damage/repair. Considerable effort is being expended in developing techniques to assess trabecular bone micro-architecture non-invasively. Site-specific bone structure information would significantly contribute to understanding the results of different therapeutic interventions, and potentially assist in optimizing the course of treatment. Three dimensional techniques that reveal trabecular bone structure are emerging as important contenders for defining bone quality, at least partially. Techniques such as micro-computed tomography have recently been developed and provide high resolution images of the trabecular architecture. A more recent development in the assessment of trabecular bone structure is the use of magnetic resonance imaging techniques that make it possible to obtain non-invasive bone biopsies at multiple anatomic sites. Cortical and trabecular bone have a low water content and short T2 and are not detectable using routine MR imaging methods. However, the marrow surrounding the trabecular bone network, if imaged at high resolution, reveals the trabecular network. Using such images, multiple different image processing and image analysis algorithms have been developed. The goal of all of these is to quantify the trabecular bone structure in 2 or 3 dimensions. The measures that have been derived so far are many, some of them synonymous with the histomorphometric measures such as trabecular bone volume fraction (BV/TV), trabecular thickness (TbTh), trabecular spacing (TbSp), trabecular number (TbN), others include connectivity or Euler number, fractal dimension, tubularity, maximal entropy, etc. A number of calibration and validation studies (in vitro and in vivo) have been undertaken in which MR-derived measures of structure are

compared with measures derived from other modalities, such as histology, micro-CT, BMD, and with biomechanics. With recent advances in phased array coils and higher strength magnets, the potential of MR imaging of bone structure is ever increasing. At the present time, the skeletal sites most commonly imaged are the radius and calcaneus. Studies currently underway are exploring the possibility of obtaining micro-architectural features of trabecular bone and the understanding whether bone turnover and micro-architecture are related, and the underlying relationship between turnover, bone mineral density and architecture, is the first step towards unraveling the therapeutic efficacy of different treatment regimens.

KEY WORDS: trabecular microarchitecture, magnetic resonance, non-invasively.

Introduction

Osteoporosis is a metabolic disorder that results in a decrease in bone mineral density and alteration in the trabecular architectural structure. Osteoporotic bone has decreased mechanical strength making it prone to fracture, especially atraumatic vertebral fractures and fall-related hip and radius fractures. Osteoporosis is clinically diagnosed using measurement of bone mineral density. Bone mineral density is usually measured using x-ray or ultrasound imaging techniques. In x-ray imaging (such as dual energy x-ray absorptiometry, DEXA, and quantitative computer tomography, QCT) the image intensity relates to the tissue mineral density. In ultrasound, image intensity reflects the change in frequency and amplitude of the sound wave traveling through the tissue. X-ray techniques use ionizing radiation, which can have deleterious effects in sufficient doses. Ultrasound, though harmless, provides only a small field of view, which may limit the accuracy of the measurement. In addition to bone density, the quality of bone which includes bone micro-architecture is of interest. Recent advances in micro-computed tomography, a x-ray based 3D technique has made it possible to obtain images of trabecular bone micro-architecture. Another promising imaging modality for measurement of trabecular architecture is magnetic resonance imaging (MRI). MRI does not use ionizing radiation and can provide three dimensional images of the bone structure. Figure 1 illustrates different imaging modalities, such as radiographs, DXA, and MRI, used to obtain images of the calcaneus and the proximal femur.

MRI basics

Nuclei with an odd number of protons and neutrons (such as hydrogen) have a magnetic moment causing the nucleus to act like a small magnet in the presence of an external magnetic field. The magnetic field of the nucleus aligns in the direction of the external magnetic field. Magnetic resonance imaging uses radio frequency (RF) pulses in a magnetic field in order to alter the spin of protons in the tissue. Coils detect the change in net magnetization, which after mathematical reconstruction pro-

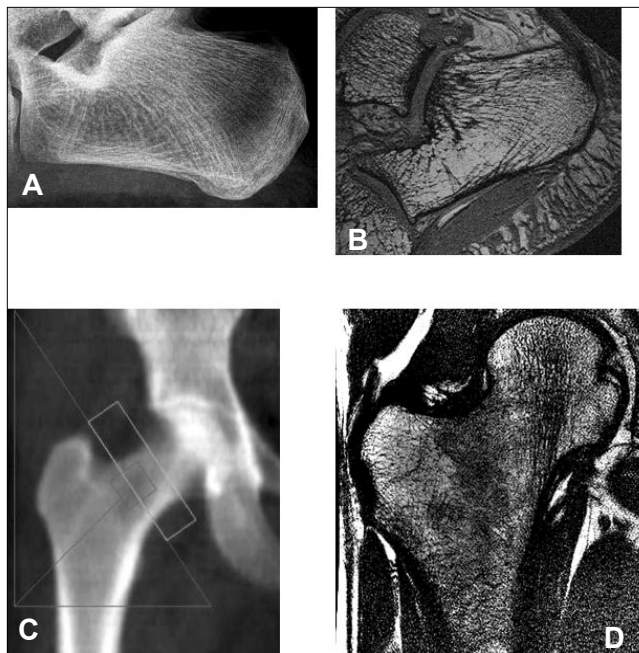


Figure 1 - Images of calcaneus using (A) radiograph and (B) MR. Image of the proximal femur using (C) DXA and (D) MR.

vides spatial and compositional information of the tissue being imaged. Because clinical MRI usually detects magnetization of hydrogen, compositional information is limited to molecules containing hydrogen, such as water, body fat, and cholesterol. In a MRI scanner, proton spins in the body align in the direction of the external magnetic field. When an RF pulse is applied, the proton spins change, altering the magnetization. The time it takes for the spins to regain its alignment with the external magnetic field after the RF pulse is turned off depends on the molecule (size and structure) and its surroundings. By altering the sequence of the RF pulses and the gradient of the magnetic field, the location and type of tissue being imaged can be controlled. The signal received in an MR image reflects intrinsic factors of the tissue, either spin density or relaxation properties of the nuclei. Spin-lattice relaxation time (T1) is the time it takes a tissue to regain longitudinal magnetization after a 90° RF pulse makes the spins perpendicular to the external magnetic field. T1 is a measure of energy transfer to the surroundings (lattice) as the proton recovers its normal spin. T1 relaxation times generally are between 300-2000 msec. Spin-spin relaxation time (T2) is a measure of how long the proton spins remain in phase after an RF pulse. Interaction with other molecules (e.g. diffusion) affects the T2 relaxation time. As natural motion of the proton increases, such as in liquids, T2 increases. Water, therefore, has a long T2, and appears white in T2-weighted images. T2 relaxation times are shorter than T1 and can range from 30-150 msec. Inhomogeneities in the magnetic field can also affect T2. A static internal field (caused by large, slow-moving proteins or rigid trabeculae for example), may additionally alter the local magnetic environment and affect T2. T2* combines the effects of molecular interactions (T2) and these field inhomogeneities. In addition to relaxation times, more complicated measures may also be obtained from the MRI signal, such as phase analysis, relaxation time distribution, and chemical composition. MR images also can reflect the behavior of water or fat alone. Figure 2 shows a radiograph of a proximal femur and a comparative fat suppressed MR image. The

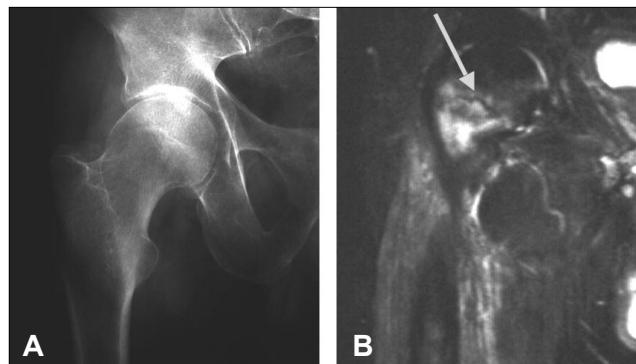


Figure 2 - (A) Radiograph and (B) fat suppressed MR image illustrating proximal femur fracture.

MR image clearly depicts the presence of a fracture.

Bone tissue has low water content, extremely short T2 and thus relatively low MR signal, and therefore appears black in most MR images. The bone marrow in trabecular bone, however, has sufficient water and fat content to provide MR signal. The trabecular bone network may alter the properties of the marrow by creating magnetic inhomogeneities at the bone-marrow interface. Trabecular structure can be imaged by relaxometry, which measures the change in marrow properties due to trabecular structure, or by direct visualization of the black trabecular network. The effect of the trabecular network on marrow magnetic properties is prominent in T2* images (1). The inhomogeneities at the bone-marrow interface are dependent on the density of the trabecular structure, the size of the trabeculae and trabecular spaces, and the field strength. In general a denser network results in shorter T2* relaxation times due to more bone-marrow interfaces and increased inhomogeneities (2-6).

The sequence and timing of RF pulses determines the image contrast. Common sequences in bone imaging include the spin-echo and gradient-echo sequences. An "echo" reverses the spin, which refocuses the magnetization and in effect cancels out external magnetic field inhomogeneities, which are intrinsic in the magnet of the scanner. In a spin-echo sequence a 90° pulse is followed by a 180° RF pulse, which produces the echo. In gradient echo sequences, the magnetic field is reversed to create the echo. The echo time (TE) is the time between the original RF pulse and the peak echo signal. The type of sequence affects the appearance of the trabecular structure. In both spin and gradient echo sequences the dimensions of the trabeculae may be amplified due to differences in magnetic susceptibility (the amount which a material becomes magnetized in a magnetic field) between the marrow and bone (7, 8). The amount of distortion artifact is dependent on TE with longer TEs resulting in more distortion (9). In addition, gradient-echo sequences produce more susceptibility artifacts than spin-echo sequences (3, 9). Representative images of the distal radius are shown in Figure 3. Spin-echo sequences, however, require a considerably longer scan time and require in-vitro samples or smaller fields of view (such as the finger and wrist) because of signal-to-noise and total imaging time considerations (8). Therefore, in vivo imaging of trabecular bone typically is performed using gradient-echo sequences with TEs as short as possible. Alternatively a fast large angle spin echo (FLASE) sequence can be used which uses an initial RF pulse greater than 90°. The following 180° pulse then partially restores the longitudinal magnetization and reduces the time to repeat (TR), making the spin-echo faster (10).

The typical maximum resolution of a 1.5T scanner is 78-200

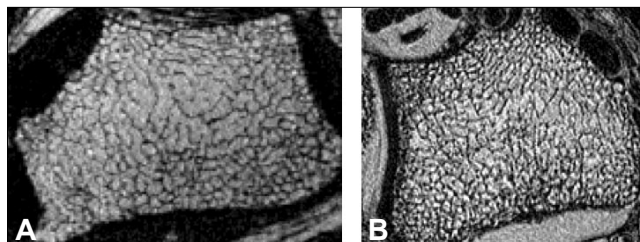


Figure 3 - Axial images of the calcaneus using (A) spin-echo and (B) gradient echo sequences.

μm in-plane and 400-1000 μm out-of-plane (slice thickness) (11). Trabeculae are the same dimensions as the in-plane resolution, resulting in partial volume effects, in which the depiction of a trabecula in the image is a projection or average of multiple trabeculae. As a result the trabecular measures obtained from MRI are different than those obtained with histomorphometry or microCT at higher resolutions (20 μm).

The magnetic field strength of the scanner affects the resolution and acquisition time of the scan. A 1.5T magnet is the standard scanner used clinically and can provide a maximum resolution of approximately 150x150x250 μm (12). With high-resolution MRI requiring a stronger magnetic field strength (7-9.4 T) and a small-bore (limited to in vitro scans), resolutions can be improved to 50x50x100 μm (8). Nuclear magnetic resonance imaging has even a smaller field of view (2-12 mm) but can obtain isotropic resolutions as high as 10 μm . NMR imaging can additionally determine chemical shift making it possible to establish distribution of a given chemical (13). Generally, higher magnetic field strength improves signal to noise ratio, scan time, and image quality, but often with limited field of view and other factors such as tissue susceptibility to consider (14).

Image processing techniques

After obtaining an MR image, pre-processing of the image is usually required in order to improve the signal-to-noise ratio and image quality and make it possible to differentiate marrow from bone trabeculae. Pre-processing may include coil correction, noise reduction, motion correction, and thresholding. Coil correction is required to correct spatial variations in the sensitivity of the detection coil as tissue close to the coil usually appears brighter than tissue further away from the coil. Coil correction algorithms depend on the structure of the specific coil. Coils that completely surround the object being scanned (e.g. bird-cage coil) provide sufficient in-plane homogeneity, making longitudinal correction sufficient. In surface coils, which may not provide in-plane homogeneity, a low-pass filter (LPF)-based coil correction scheme is necessary (15, 16) (Figure 4). Noise reduction improves the signal-to-noise ratio and may be accomplished using a median low pass filter, in which the median of the pixels in a certain kernel size (e.g. 3x3 pixels) surrounding a pixel becomes the new filtered value for the pixel (11). A low pass filter removes high signal noise, while preserving the low signal data. The kernel median allows edge detection, whereas the kernel mean would smooth the data and blur the edges. Hwang et al. proposed a histogram deconvolution method in order to obtain a noiseless histogram for trabecular bone (17). In this method a probability distribution of the noise (e.g. Gaussian) and an initial estimate of the noiseless histogram are assumed in order to predict a histogram. The predicted histogram is iteratively im-

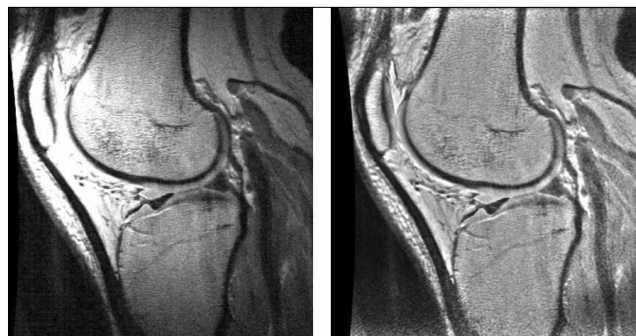


Figure 4 - Effects of coil correction on sagittal images of the calcaneus. Coil correction equalizes the fat and marrow intensities throughout the visible bone.

proved by comparing it to the measured histogram. The noiseless histogram and raw image are used to produce a noiseless image. Others have proposed wavelet-based thresholding that allows more local noise reduction while retaining relevant detail information (18-20).

Imaging trabeculae on the order of 100 μm means that a small amount of motion will affect the image. Various techniques have been devised to correct for motion artifacts. Navigator correction alters the echo sequence, adding echoes to sense small displacements (21). The data is corrected in k-space by analyzing the phase shift and adjusting for translational motions. Studies have shown that navigator correction improves reproducibility and accuracy of trabecular bone parameters (22). Retrospective motion correction can also be performed with autofocus (23, 24) (Figure 5). This technique applies total phase shifts to the data and compares the resulting image with the original. An entropy focusing criterion is applied to minimize the amount of entropy in the image and obtain maximum contrast.

Perhaps the most critical pre-processing step is thresholding, which allows delineation of the trabeculae and the marrow. Because the resolution of in vivo MR images is on the same scale as the trabecular width, partial volume effects occur. In partial voluming, a single voxel may contain signals from multiple tissue types. The voxel intensity is the average signal from the various tissues. The histogram of trabecular bone, therefore, is not bi-modal with marrow and bone peaks, but rather mono-



Figure 5 - Coronal images of the shoulder. A. Original image corrupted by motion. B. After motion correction (From Atkinson et al., *Magnetic Resonance in Medicine* 1999;41(1):169. Reprinted with permission of Wiley-Liss Inc., a subsidiary of John Wiley & Sons Inc., Copyright 1999).

modal with a peak intensity between the values of marrow and bone. Various thresholding methods have been established in order to segment the bone from the marrow where partial volume effects are an issue. Majumdar et al. proposed a dual thresholding method in which the threshold for bone was a mean pixel value taken in the cortical shell and the threshold for marrow was the lower signal intensity at which the histogram reached half its peak (11).

Link et al. compared global and local thresholding methods (25). Global thresholding applies the same threshold throughout the entire image. The disadvantage of global thresholding is that images of with a dense trabecular structure appear completely black, while images with a sparse trabecular structure appear white. Using local thresholding the intensity of a square region surrounding a pixel is averaged. If the central pixel has an intensity lower than the average, it is considered bone; higher than average pixels are considered marrow. Local thresholding is not affected by bone density, but is dependent on noise in the image. It was found that global thresholding was more accurate in calculating trabecular thickness and local thresholding was more accurate in predicting trabecular spacing.

Wu et al. introduced a Bayesian approach to segment bone from marrow in which each voxel was divided into subvoxels (26). The local tissue environment influenced the distribution of bone and marrow within the subvoxels with a Gibbs distribution modeling the interaction between subvoxels. This approach improves segmentation but has only been performed on images from small-bore NMR microscopy machines and has yet to be applied to clinical scans. Hwang et al. proposed a spatial autocorrelation analysis which also used the local tissue environment to determine the probability of finding bone at specific locations (27). This method was used to analyze images at in vivo resolution (voxel size of $156 \times 156 \times 311 \mu\text{m}^3$). Similarly, a relaxation labeling process that takes into account the spatial context, in particular local contextual information (e.g. in Markov fields) was used by Antoniadis et al. to segment trabecular bone (28). Each pixel was assigned a probability of being bone or marrow and then iteratively updated according to the local and surrounding segments until the probability of each pixel was either 1 or 0. Thresholding using one of these techniques results in a binarized image that consists of only bone or marrow voxels.

Post-processing: architectural parameters

Bone mineral density and trabecular structure together determine the mechanical strength of trabecular bone. The main objective of imaging trabecular bone structure is to determine morphological parameters of the trabecular architecture. These morphologic parameters may help to determine the efficacy of therapeutic treatments for osteoporosis and predict individuals at risk for bone fracture. Standard histomorphometric measures of bone structure include: bone volume fraction (BV/TV), trabecular thickness (Tb.Th), mean intercept length, trabecular number (Tb.N), and trabecular spacing (Tb.S). These parameters have been adapted to analyze MR images of trabecular structure.

Because the resolution of in vivo MR images is on the same scale as trabecular dimensions, these histomorphometric parameters are the measures of the trabeculae projected across the slice thickness. Majumdar et al. introduced "apparent" measures, indicating that the morphometric measures obtained from in vivo MR images may not be exactly equivalent, however are related to those obtained from higher resolution modalities (11). It was found that trabecular spacing and trabecular

number are relatively independent of resolution (29). Trabecular thickness, however, was strongly dependent on resolution with lower resolutions resulting in thicker trabeculae.

A 3 dimensional distance technique was introduced by Hildebrand and Rüeggsegger to determine mean thickness by fitting spheres within the structure (30). This measure was able to distinguish between trabecular bone composed of a greater percentage of plates or rods (30). It has also been used calculate histomorphometric parameters such as app.Tb.Th and app.Tb.Sp from MR images (14, 31). The morphological parameters calculated using the distance technique correlated well with those calculated using the mean intercept length (14).

Because osteoporosis is thought to result in a thinning of trabeculae and loss of trabecular connectivity, measures of connectivity are important in determining osteoporotic bone quality. Connectivity measures have been established to measure the degree of connectivity of the trabecular network in trabecular bone (32, 33). Connectivity indicates the maximum number of branches that can be broken before the structure is separated into two parts. It is a topological invariant, which means it does not change if the structure is stretched, bent, twisted or other rubber-like deformation. Connectivity can be calculated in terms of the Euler characteristic. Previous studies have used the Euler number to analyze MR images of trabecular bone and found that connectivity can vary between regions within a bone (34) and is significantly correlated with bone density and bone volume fraction (9, 35, 36).

Fractal dimensions are a measure of the self-similarity of a structure over different scales and have also been used to characterize trabecular architecture. Fractal dimension (D) can be determined using a box-counting technique in which a grid of boxes is superimposed on the trabecular structure (37-39). The number of boxes (N) that contain trabeculae is determined for various sizes (ϵ) of grids. Others have used analysis based on Brownian motion to estimate the Hurst exponent (H), which indicates if the structure is random or contains patterns, and derived the fractal dimension from H (40). Studies found that fractal dimension decreased with age (11, 37), was significantly lower in patients with vertebral compression fracture (37) and hip fracture, (41, 42) and was not correlated with bone mineral density (41, 43). Interestingly it was found that fractal dimension was not different between those with osteopenia and osteoporosis, but was nonetheless an independent predictor of bone failure strength (43). It has been proposed that a decrease in fractal dimension is related to a disorganization of trabecular architecture and loss of connectivity (40).

Pothuau et al. proposed further classification of the trabecular architecture using a skeleton graph of the trabecular network (44, 45). The skeleton graph preserved topographical equivalence with the original network, meaning the connectivity did not change as the trabeculae were thinned to 1 pixel width. This method provides further insight into the influence of connectivity on overall trabecular structure. Others went on to classify the connectivity in terms of curves, surfaces, and junctions of the two (46, 47). They found that parameters from this digital topological analysis correlated well with bone volume fraction and measures of mechanical integrity, such as Young's modulus.

Trabecular bone structure is anisotropic, and architectural measures may, therefore, differ depending on the orientation. Spatial autocorrelation analysis (48, 49) is a method to quantify not only the distance between trabeculae, but also how this varies with respect to orientation (i.e. the amount of anisotropy). The autocorrelation function (ACF) is a measure of the probability of finding bone n pixels away from a certain pixel and is equal to the product of the bone volume fractions for

the two pixels. Parameters derived from the ACF provide measures of the structure's alignment perpendicular to the slice plane (tubularity) and distribution within the slice plane (transverse contiguity). One advantage of autocorrelation analysis is that it does not depend on thresholding or binarizing the images into bone and marrow. It was found that ACF measures of anisotropy correlate well with Young's modulus and are different for normal and osteoporotic trabecular bone (27, 48). The scaling index method (SIM) has also been used to measure non-linear structural information from non-binarized trabecular bone images (50). The scaling index (α) is a measure of the isotropy of the structure with larger values of α indicating a more random structure. The scaling index correlated better with mechanical strength and BMD than traditional histomorphometric measures.

Comparison with other imaging modalities

Several studies have explored how MR images compare with other imaging modalities in determining structural parameters (Table I). Hipp et al. and Hopper et al. used small-bore MRI with resolutions of $92 \times 92 \times 92 \mu\text{m}^3$ and $23 \times 23 \times 39 \mu\text{m}^3$ respectively (51, 52). All other studies were performed on 1.5 or 3T scanners with in-plane resolution of 100-150 μm and a slice thickness of 300 μm on in vitro bone cubes. Weber et al. compared MR in vivo and in vitro trabecular bone images from mice with histological sections (53). They found parameters derived from in vivo images correlated better with histological parameters than did in vitro images and attributed the difference to the better MR signal from bone marrow than formalin. These studies indicate that MR derived architectural parameters correlate well with measures taken at much higher resolutions. In general, MR tended to overestimate BV/TV and Tb.Th and underestimate Tb.Sp due to partial volume effects.

Architectural parameters have also been compared to bone mineral density (BMD) and mechanical strength in the radius, (43) lumbar vertebrae (54), femur (45), calcaneus (56) and among various sights (36). In these studies correlations coeffi-

cients for BV/TV, Tb.Th, and Tb.N with BMD or mechanical strength were between 0.5 and 0.8. All studies found that Tb.Sp had a correlation coefficient with BMD or mechanical strength of -0.5 to -0.6, indicating that the spacing between the trabeculae increases as BMD and mechanical strength decrease. Studies also found that combining BMD and trabecular structural parameters improved correlations with mechanical strength.

In vivo imaging in humans

DXA is the gold standard for diagnosing osteoporotic bone, however only provides an areal measure of bone mineral density. Multi-slice CT can be used for volumetric bone mineral density and structural measurements. Though MR cannot provide measures of BMD, it can provide trabecular bone structural measures and does not require radiation. Trabecular bone structure also varies considerably depending on the skeletal site, as well as within a given skeletal site (Figure 6). Studies have examined the trabecular structure in the calcaneus of normal and osteoporotic women and found that structural parameters (especially BV/TV, Tb.Sp, Tb.N, and connectivity measures) were significantly different between normals and osteoporotic trabecular bone (41, 57, 58). The same was found to be true in the calcaneus of normal and osteoporotic men (59) and in the radius of premenopausal, postmenopausal normal, and postmenopausal patients with hip fractures (10). Tb.Sp demonstrated that largest change with age, increasing significantly in postmenopausal women with hip fractures. Benito et al. detected bone loss in hypogonadal men using MR (60). They found that the ratio of plates to rod (surface voxels to curve voxels in their analysis) and bone volume fraction decreased in hypogonadal men. Correspondingly, the erosion index, a combination of topological parameters that increases as bone architecture deteriorates, was higher in men with hypogonadism.

MR has been used to measure structural bone changes in steroid induced osteoporosis in patients after renal and cardiac transplantation (61). Structural parameters were significantly lower (except for Tb.Sp, which was higher) after cardiac transplantation

Table I - Correlation of MR derived trabecular parameters with those derived from other imaging modalities. All values are statistically significant with $p < 0.05$. n.s. denotes correlations that were not statistically significant.

Imaging Modality	Bone Type	Correlation coefficients				Reference
		BV/TV	Tb.Sp	Tb.N	Tb.Th	
X-ray tomographic microscopy (18 μm)	Distal radius	n.s.	n.s.	n.s.	0.87	77
Optical images (23 μm)	Bovine (various)	0.9	0.85	0.73	-	51
Optical images (20 μm)	Calcaneus, femur	0.69	0.89	0.78	n.s.	36
Scanning electron microscopy (20x)	Rat femur	0.72	0.82	0.91	0.89	52
Macro section radiograph (5 μm)	Distal radius	0.67	0.59	n.s.	0.66	78
Macro section radiograph (5 μm)	Calcaneus	0.63	0.58	n.s.	0.68	79
CT (247x247x1000 μm^3)	Distal radius	0.72	0.49	0.47	0.57	78
MicroCT (22 μm)	Femoral head	0.9	0.92	.90	.82	14

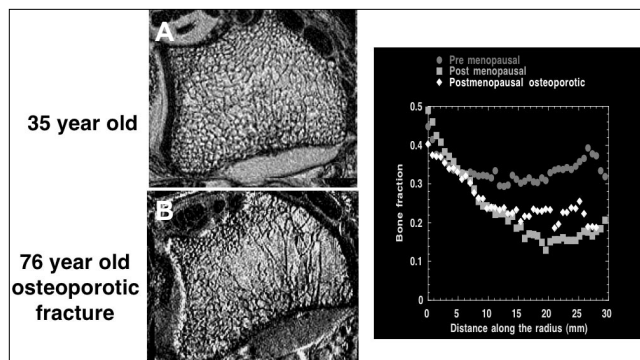


Figure 6 - Axial MR images of the distal radius (156x156x500 μm). A. Non-osteoporotic 37 year old. B. Osteoporotic 76 year old with radial fracture. Note the thinning of the trabeculae and loss of trabecular bone volume. The figure on the right illustrates pre and post-menopausal decrease in bone fraction in the radius as one moves from the joint line into the shaft.

due to the altered bone metabolism caused by immunosuppressive drugs. Large pre- and post-transplant differences in structural parameters were not seen in renal patients probably because renal failure can alter bone metabolism and trabecular structure before transplantation occurs. Chesnut et al. have published the first longitudinal study showing that nasal spray calcitonin preserves trabecular bone micro-architecture in the distal radius (62).

Imaging in animal studies

MR also has been used to measure structural parameters in animal models of osteoporosis. Jiang et al. treated an ovariectomized sheep model of osteoporosis with salmon calcitonin, an osteoclast inhibitor, to determine if structural parameters in the neck of the femur could be maintained (63). It was found that BV/TV and Tb N decreased and Tb Sp increased in ovariectomized sheep. Structural parameters of sheep treated with salmon calcitonin were equivalent to sham operated sheep. Small-bore micro-MRI has been used to study osteoporotic bone structure in ovariectomized rats (64). Analysis of MR images revealed differences in osteoporotic trabecular structure that DXA could not detect.

Takahashi et al. have investigated the effects of corticosteroid on bone structure in rabbit femurs using magnetic resonance microimaging (μMRI) (65). They found that short term, high doses of corticosteroids resulted in a decrease in trabecular bone volume through trabecular thinning with little change in trabecular network, trabecular number or trabecular spacing. Using MR spectroscopy they also determined that hematopoietic bone marrow was converted to fatty marrow in rabbits treated with corticosteroid.

Future

Recent advances in micro-CT imaging *in vivo* (66, 67) make it possible to obtain radius and tibia images using this methodology. However, comparative studies, *in-vivo* case-control studies, longitudinal studies using micro-CT *in vivo* in humans have not been undertaken and are clearly warranted. MR imaging has proved to be a valid method for analyzing trabecular structure and offers distinct advantages over other imaging modalities. Besides being non-ionizing, and providing the ability to image skeletal sites such as the calcaneus, hip, tibia, femur, it offers the advantages of characterizing bone and the adjoining soft tissues. In particular, MR images soft tissue, such as cartilage, muscle,

marrow, and meniscus, which is not possible with x-ray based imaging modalities. Understanding the relationship between bone and cartilage is critical, particularly in cases of arthritis or injury. It has been found that degradation of cartilage on one compartment of the knee corresponds with a loss of trabecular structure in the other compartment, which is probably linked to mechanical load between the compartments (54, 68).

Most MR images display proton signals from water or fat. It is possible, however, to detect signals from other molecules in a technique called MR spectroscopy. This technique has been used to a limited amount in bone imaging, in particular to image phosphorus in cortical and trabecular bone (69) and lipids in the red bone marrow in hematological diseases (70). It has also been suggested that MRI can be used to detect the increase in lipid-to-water ratio in the vertebral bodies in patients with osteoporosis (71).

The combination of MR imaging and finite element (FE) analysis has been used to determine mechanical properties of trabecular bone (72-74). This allows the *in vivo* estimation of mechanical properties, which are usually determined by *in vitro* compression testing. In FE models derived from MR images it is possible to incorporate soft tissue structures in the model. This would be useful not only in mechanobiological models of tissue differentiation and bone remodeling (75), but also in models of fracture healing where cartilage formation is critical to the process (76).

Bone quality has been an emerging concept in the area of osteoporosis. Trabecular bone micro-architecture, bone geometry and associated marrow changes in osteoporosis can all be probed using MRI. Thus, MR techniques have the potential for providing a complete whole organ assessment of skeletal status in osteoporosis, and further developments in this imaging modality and research studies are clearly warranted.

References

1. Davis CA, Genant HK, Dunham JS. The effects of bone on proton NMR relaxation times of surrounding liquids. *Invest Radiol*. 1986; 21:472-7.
2. Brismar TB, Hindmarsh T, Ringertz H. Experimental correlation between $T2^*$ and ultimate compressive strength in lumbar porcine vertebrae. *Acad Radiol*. 1997;4:426-30.
3. Majumdar S. Quantitative study of the susceptibility difference between trabecular bone and bone marrow: computer simulations. *Magn Reson Med*. 1991;22:101-10.
4. Brismar TB, Karlsson M, Li T, Ringertz H. The correlation between $R2'$ and bone mineral measurements in human vertebrae: an *in vitro* study. *Eur Radiol*. 1999;9:141-4.
5. Kang C, Paley M, Ordidge R, Speller R. $R2'$ measured in trabecular bone *in vitro*: relationship to trabecular separation. *Magn Reson Imaging*. 1999;17:989-95.
6. Majumdar S, Genant HK. *In vivo* relationship between marrow $T2^*$ and trabecular bone density determined with a chemical shift-selective asymmetric spin-echo sequence. *J Magn Reson Imaging*. 1992;2:209-19.
7. Bakker CJ, Bhagwandien R, Moerland MA, Ramos LM. Simulation of susceptibility artifacts in 2D and 3D Fourier transform spin-echo and gradient-echo magnetic resonance imaging. *Magn Reson Imaging*. 1994;12:767-74.
8. Jara H, Wehrli FW, Chung H, Ford JC. High-resolution variable flip angle 3D MR imaging of trabecular microstructure *in vivo*. *Magn Reson Med*. 1993;29:528-39.
9. Majumdar S, Newitt D, Jergas M, Gies A, Chiu E, Osman D, Keltner J, Keyak J, Genant H. Evaluation of technical factors affecting the quantification of trabecular bone structure using magnetic resonance imaging. *Bone*. 1995;17:417-30.
10. Ma J, Wehrli FW, Song HK. Fast 3D large-angle spin-echo imaging (3D FLASE). *Magn Reson Med*. 1996;35:903-10.

11. Majumdar S, Genant HK, Grampp S, Newitt DC, Truong VH, Lin JC, Mathur A. Correlation of trabecular bone structure with age, bone mineral density, and osteoporotic status: in vivo studies in the distal radius using high resolution magnetic resonance imaging. *J Bone Miner Res.* 1997;12:111-8.
12. Link TM, Majumdar S, Grampp S, Guglielmi G, van Kuijk C, Imhof H, Glueer C, Adams JE. Imaging of trabecular bone structure in osteoporosis. *Eur Radiol.* 1999;9:1781-8.
13. Timonen J, Alvila L, Hirva P, Pakkanen TT. Nuclear magnetic resonance imaging - a potential method for analysis of bone material. *J Mater Sci Mater Med.* 1998;9:187-90.
14. Sell CA, Masi JN, Burghardt A, Newitt D, Link TM, Majumdar S. Quantification of Trabecular Bone Structure Using Magnetic Resonance Imaging at 3 Tesla-Calibration Studies Using Microcomputed Tomography as a Standard of Reference. *Calcif Tissue Int.* 2005.
15. Newitt D, Majumdar S. Correction for receiver coil inhomogeneity profiles for quantitative analysis of trabecular bone structure from high resolution MRI. *Proceedings from 7th ISMRM*, pp. 1046. Philadelphia; 1999.
16. Newitt DC, van Rietbergen B, Majumdar S. Processing and analysis of in vivo high-resolution MR images of trabecular bone for longitudinal studies: reproducibility of structural measures and micro-finite element analysis derived mechanical properties. *Osteoporos Int.* 2002;13:278-87.
17. Hwang SN, Wehrli FW. Estimating voxel volume fractions of trabecular bone on the basis of magnetic resonance images acquired in vivo. *Int J Imaging Syst Technol.* 1999;10:18-198.
18. Wink AM, Roerdink JB. Denoising functional MR images: a comparison of wavelet denoising and Gaussian smoothing. *IEEE Trans Med Imaging.* 2004;23:374-87.
19. Scheunders P. Wavelet thresholding of multivalued images. *IEEE Trans Image Process.* 2004;13:475-83.
20. Bao P, Zhang L. Noise reduction for magnetic resonance images via adaptive multiscale products thresholding. *IEEE Trans Med Imaging.* 2003;22:1089-99.
21. Ehman RL, Felmlee JP. Adaptive technique for high-definition MR imaging of moving structures. *Radiology.* 1989;173:255-63.
22. Song HK, Wehrli FW. In vivo micro-imaging using alternating navigator echoes with applications to cancellous bone structural analysis. *Magn Reson Med.* 1999;41:947-53.
23. Atkinson D, Hill DL, Stoyke PN, Summers PE, Clare S, Bowtell R, Keevil SF. Automatic compensation of motion artifacts in MRI. *Magn Reson Med.* 1999;11:163-70.
24. Atkinson D, Hill DL, Stoyke PN, Summers PE, Keevil SF. Automatic correction of motion artifacts in magnetic resonance images using an entropy focus criterion. *IEEE Trans Med Imaging.* 1997;16:903-10.
25. Link TM, Majumdar S, Lin JC, Augat P, Gould RG, Newitt D, Ouyang X, Lang TF, Mathur A, Genant HK. Assessment of trabecular structure using high resolution CT images and texture analysis. *J Comput Assist Tomogr.* 1998;22:15-24.
26. Wu Z, Chung HW, Wehrli FW. A Bayesian approach to subvoxel tissue classification in NMR microscopic images of trabecular bone. *Magn Reson Med.* 1994;31:302-8.
27. Hwang SN, Wehrli FW, Williams JL. Probability-based structural parameters from three-dimensional nuclear magnetic resonance images as predictors of trabecular bone strength. *Med Phys.* 1997;24:1255-61.
28. Antoniadis T, Scarpelli JP, Ruaud JP, Gonord P, Guillot G. Bone labelling on micro-magnetic resonance images. *Med Image Anal.* 1999;3:119-28.
29. Kothari M, Keaveny TM, Lin JC, Newitt DC, Genant HK, Majumdar S. Impact of spatial resolution on the prediction of trabecular architecture parameters. *Bone.* 1998;22:437-43.
30. Hildebrand T, Rueggsegger P. A new method for the model-independent assessment of thickness in three-dimensional images. *J Microsc.* 1997;185:67-75.
31. Laib A, Newitt DC, Lu Y, Majumdar S. New model-independent measures of trabecular bone structure applied to in vivo high-resolution MR images. *Osteoporos Int.* 2002;13:130-6.
32. Odgaard A, Gundersen HJ. Quantification of connectivity in cancellous bone, with special emphasis on 3-D reconstructions. *Bone.* 1993;14:173-82.
33. Feldkamp LA, Goldstein SA, Parfitt AM, Jesion G, Kleerekoper M. The direct examination of three-dimensional bone architecture in vitro by computed tomography. *J Bone Miner Res.* 1989;4:3-11.
34. Stampa B, Kuhn B, Liess C, Heller M, Glueer CC. Characterization of the integrity of three-dimensional trabecular bone microstructure by connectivity and shape analysis using high-resolution magnetic resonance imaging in vivo. *Top Magn Reson Imaging.* 2002;13:357-63.
35. Majumdar S, Genant HK. Assessment of trabecular structure using high resolution magnetic resonance imaging. *Stud Health Technol Inform.* 1997;40:81-96.
36. Majumdar S, Kothari M, Augat P, Newitt DC, Link TM, Lin JC, Lang T, Lu Y, Genant HK. High-resolution magnetic resonance imaging: three-dimensional trabecular bone architecture and biomechanical properties. *Bone.* 1998;22:445-54.
37. Weinstein RS, Majumdar S. Fractal geometry and vertebral compression fractures. *J Bone Miner Res.* 1994;9:1797-802.
38. Majumdar S, Weinstein RS, Prasad RR. Application of fractal geometry techniques to the study of trabecular bone. *Med Phys.* 1993;20:1611-9.
39. Chung HW, Chu CC, Underweiser M, Wehrli FW. On the fractal nature of trabecular structure. *Med Phys.* 1994;21:1535-40.
40. Pothuau L, Benhamou CL, Porion P, Lespessailles E, Harba R, Levitz P. Fractal dimension of trabecular bone projection texture is related to three-dimensional microarchitecture. *J Bone Miner Res.* 2000;15:691-9.
41. Link TM, Majumdar S, Augat P, Lin JC, Newitt D, Lu Y, Lane NE, Genant HK. In vivo high resolution MRI of the calcaneus: differences in trabecular structure in osteoporosis patients. *J Bone Miner Res.* 1998;13:1171-81.
42. Majumdar S, Lin JC, Millard J, Lin JC, Augat P, Newitt D, Lane NE, Genant HK. In vivo assessment of trabecular bone structure using fractal analysis of distal radius radiographs. *Med Phys.* 2000;27:2594-9.
43. Hudelmaier M, Kollstedt A, Lochmuller EM, Kuhn V, Eckstein F, Link TM. Gender differences in trabecular bone architecture of the distal radius assessed with magnetic resonance imaging and implications for mechanical competence. *Osteoporos Int.* 2005.
44. Pothuau L, Porion P, Lespessailles E, Benhamou CL, Levitz P. A new method for three-dimensional skeleton graph analysis of porous media: application to trabecular bone microarchitecture. *J Microsc.* 2000;199 (Pt 2):149-61.
45. Pothuau L, Newitt DC, Lu Y, MacDonald B, Majumdar S. In vivo application of 3D-line skeleton graph analysis (LSGA) technique with high-resolution magnetic resonance imaging of trabecular bone structure. *Osteoporos Int.* 2004;15:411-9.
46. Gomberg BR, Saha PK, Song HK, Hwang SN, Wehrli FW. Topological analysis of trabecular bone MR images. *IEEE Trans Med Imaging.* 2000;19:166-74.
47. Wehrli FW, Gomberg BR, Saha PK, Song HK, Hwang SN, Snyder PJ. Digital topological analysis of in vivo magnetic resonance microimages of trabecular bone reveals structural implications of osteoporosis. *J Bone Miner Res.* 2001;16:1520-31.
48. Rotter M, Berg A, Langenberger H, Grampp S, Imhof H, Moser E. Autocorrelation analysis of bone structure. *J Magn Reson Imaging.* 2001;14:87-93.
49. Wehrli FW, Saha PK, Gomberg BR, Song HK, Snyder PJ, Benito M, Wright A, Weening R. Role of magnetic resonance for assessing structure and function of trabecular bone. *Top Magn Reson Imaging.* 2002;13:335-55.
50. Boehm HF, Raeth C, Monetti RA, Mueller D, Newitt D, Majumdar S, Rummey E, Morfill G, Link TM. Local 3D scaling properties for the analysis of trabecular bone extracted from high-resolution magnetic resonance imaging of human trabecular bone: comparison with bone mineral density in the prediction of biomechanical strength in vitro. *Invest Radiol.* 2003;38:269-80.
51. Hipp JA, Jansujwicz A, Simmons CA, Snyder BD. Trabecular bone

- morphology from micro-magnetic resonance imaging. *J Bone Miner Res.* 1996;11:286-97.
52. Hopper TA, Meder R, Pope JM. Comparison of high-resolution MRI, optical microscopy and SEM for quantitation of trabecular architecture in the rat femur. *Magn Reson Imaging.* 2004;22:953-61.
 53. Weber MH, Sharp JC, Latta P, Sramek M, Hassard HT, Orr FW. Magnetic resonance imaging of trabecular and cortical bone in mice: comparison of high resolution in vivo and ex vivo MR images with corresponding histology. *Eur J Radiol.* 2005;53:96-102.
 54. Beuf O, Newitt DC, Mosekilde L, Majumdar S. Trabecular structure assessment in lumbar vertebrae specimens using quantitative magnetic resonance imaging and relationship with mechanical competence. *J Bone Miner Res.* 2001;16:1511-9.
 55. Link TM, Vieth V, Langenberg R, Meier N, Lotter A, Newitt D, Majumdar S. Structure analysis of high resolution magnetic resonance imaging of the proximal femur: in vitro correlation with biomechanical strength and BMD. *Calcif Tissue Int.* 2003;72:156-65.
 56. Ouyang X, Selby K, Lang P, Engelke K, Klifa C, Fan B, Zucconi F, Hottya G, Chen M, Majumdar S, Genant HK. High resolution magnetic resonance imaging of the calcaneus: age-related changes in trabecular structure and comparison with dual X-ray absorptiometry measurements. *Calcif Tissue Int.* 1997;60:139-47.
 57. Herlidou S, Grebe R, Grados F, Leuyer N, Fardellone P, Meyer ME. Influence of age and osteoporosis on calcaneus trabecular bone structure: a preliminary in vivo MRI study by quantitative texture analysis. *Magn Reson Imaging.* 2004;22:237-43.
 58. Link TM, Bauer J, Kollstedt A, Stumpf I, Hudelmaier M, Settles M, Majumdar S, Lochmuller EM, Eckstein F. Trabecular bone structure of the distal radius, the calcaneus, and the spine: which site predicts fracture status of the spine best? *Invest Radiol.* 2004;39: 487-97.
 59. Boutry N, Cortet B, Dubois P, Marchandise X, Cotten A. Trabecular bone structure of the calcaneus: preliminary in vivo MR imaging assessment in men with osteoporosis. *Radiology.* 2003;227: 708-17.
 60. Benito M, Gomberg B, Wehrli FW, Weening RH, Zemel F, Wright AC, Song HK, Cucchiara A, Snyder PJ. Deterioration of trabecular architecture in hypogonadal men. *J Clin Endocrinol Metab.* 2003; 88:1497-502.
 61. Link TM. High-resolution magnetic resonance imaging to assess trabecular bone structure in patients after transplantation: a review. *Top Magn Reson Imaging.* 2002;13:363-75.
 62. Chesnut CH, Majumdar S, Newitt D, Shields A, Van Pelt J, Laschansky E, Azria M, Kriegerman A, Olson M, Erikson E, Mindeholm L. Effects of salmon calcitonin on trabecular microarchitecture as determined by magnetic resonance imaging: results from the Quest study. *J Bone Miner Res.* (epub) April; 2005.
 63. Jiang Y, Zhao J, Geusens P, Liao EY, Adriaensens P, Gelan J, Azria M, Boonen S, Caulin F, Lynch JA, Ouyang X, Genant HK. Femoral neck trabecular microstructure in ovariectomized ewes treated with calcitonin: MRI microscopic evaluation. *J Bone Miner Res.* 2005;20:125-30.
 64. Jiang Y, Zhao J, White DL, Genant HK. Micro CT and Micro MR imaging of 3D architecture of animal skeleton. *J Musculoskelet Neuronal Interact.* 2000;1:45-51.
 65. Takahashi M, Wehrli FW, Hilaire L, Zemel BS, Hwang SN. In vivo NMR microscopy allows short-term serial assessment of multiple skeletal implications of corticosteroid exposure. *Proc Natl Acad Sci USA.* 2002;99:4574-9.
 66. Laib A, Hammerle S, Koller B. A New 100 µm Resolution Scanner for in vivo 3D-CT of the Human Forearm and Lower Leg. 16th Annual Bone Densitometry Workshop. Annecy, France; 2004.
 67. Boutroy S, Bouxsein M, Munoz F, Delmas P. In Vivo Assessment of Trabecular Microarchitecture by High-Resolution Peripheral Quantitative Computed Tomography. *JCEM*; 2005 in press.
 68. Lindsey CT, Narasimhan A, Adolfo JM, Jin H, Steinbach LS, Link T, Ries M, Majumdar S. Magnetic resonance evaluation of the interrelationship between articular cartilage and trabecular bone of the osteoarthritic knee. *Osteoarthritis Cartilage.* 2004;12:86-96.
 69. Robson MD, Gatehouse PD, Bydder GM, Neubauer S. Human imaging of phosphorus in cortical and trabecular bone in vivo. *Magn Reson Med.* 2004;51:888-92.
 70. Schick F, Einsele H, Kost R, Duda SH, Horny HP, Lutz O, Claussen CD. Localized MR 1H spectroscopy reveals alterations of susceptibility in bone marrow with hemosiderosis. *Magn Reson Med.* 1994;32:470-5.
 71. Lin CS, Fertikh D, Davis B, Lauerman WC, Henderson F, Schellinger D. 2D CSI proton MR spectroscopy of human spinal vertebra: feasibility studies. *J Magn Reson Imaging.* 2000;11:287-93.
 72. Pothuau L, Van Rietbergen B, Mosekilde L, Beuf O, Leuyer N, Benhamou CL, Majumdar S. Combination of topographic parameters and bone volume fraction better predicts the mechanical properties of trabecular bone. *J Biomech.* 2002;35:1091-9.
 73. Newitt DC, Majumdar S, van Rietbergen B, von Ingersleben G, Harris ST, Genant HK, Chesnut C, Garnero P, MacDonald B. In vivo assessment of architecture and micro-finite element analysis derived indices of mechanical properties of trabecular bone in the radius. *Osteoporos Int.* 2002;13:6-17.
 74. van Rietbergen B, Majumdar S, Newitt D, MacDonald B. High-resolution MRI and micro-FE for the evaluation of changes in bone mechanical properties during longitudinal clinical trials: application to calcaneal bone in postmenopausal women after one year of idoxifene treatment. *Clin Biomech (Bristol, Avon)* 2002;17:81-8.
 75. Shefelbine SJ, Augat P, Claes L, Simon U. Trabecular bone fracture healing simulation with finite element analysis and fuzzy logic. *Journal of Biomechanics*; in press.
 76. Shefelbine SJ, Simon U, Claes L, Gold A, Gabet Y, Bab I, Muller R, Augat P. Prediction of fracture callus mechanical properties using micro-CT images and voxel-based finite element analysis. *Bone.* 2005;36:480-8.
 77. Majumdar S, Newitt D, Mathur A, Osman D, Gies A, Chiu E, Lotz J, Kinney J, Genant H. Magnetic resonance imaging of trabecular bone structure in the distal radius: relationship with X-ray tomo-

- graphic microscopy and biomechanics. *Osteoporos Int.* 1996;6: 376-85.
78. Link TM, Vieth V, Stehling C, Lotter A, Beer A, Newitt D, Majumdar S. High-resolution MRI vs multislice spiral CT: which technique depicts the trabecular bone structure best? *Eur Radiol.* 2003;13: 663-71.
79. Vieth V, Link TM, Lotter A, Persigehl T, Newitt D, Heindel W, Majumdar S. Does the trabecular bone structure depicted by high-resolution MRI of the calcaneus reflect the true bone structure? *Invest Radiol.* 2001;36:210-7.

FOR REVIEW ONLY
© CIC EDIZIONI INTERNAZIONALI